◆ Human Brain Mapping 38:957–973 (2017) ◆

Dynamic Functional Network Connectivity in Idiopathic Generalized Epilepsy with Generalized Tonic–Clonic Seizure

Feng Liu,[1,2] Yifeng Wang,[1] Meiling Li,[1] Wenqin Wang,[3] Rong Li,[1] Zhiqiang Zhang,[4] Guangming Lu,[4]* and Huafu Chen[1]*

[1]Key Laboratory for NeuroInformation of Ministry of Education, School of Life Science and Technology and Center for Information in BioMedicine, University of Electronic Science and Technology of China, Chengdu, Sichuan, 610054, People's Republic of China
[2]Department of Radiology and Tianjin Key Laboratory of Functional Imaging, Tianjin Medical University General Hospital, Tianjin, 300052, People's Republic of China
[3]School of Sciences, Tianjin Polytechnic University, Tianjin, 300130, People's Republic of China
[4]Department of Medical Imaging, Jinling Hospital, Nanjing University School of Medicine, Nanjing, 210002, People's Republic of China

Abstract: Idiopathic generalized epilepsy (IGE) has been linked with disrupted intra-network connectivity of multiple resting-state networks (RSNs); however, whether impairment is present in inter-network interactions between RSNs, remains largely unclear. Here, 50 patients with IGE characterized by generalized tonic–clonic seizures (GTCS) and 50 demographically matched healthy controls underwent resting-state fMRI scans. A dynamic method was implemented to investigate functional network connectivity (FNC) in patients with IGE-GTCS. Specifically, independent component analysis was first carried out to extract RSNs, and then sliding window correlation approach was employed to obtain dynamic FNC patterns. Finally, *k*-mean clustering was performed to characterize six discrete functional connectivity states, and state analysis was conducted to explore the potential alterations in FNC and other dynamic metrics. Our results revealed that state-specific FNC disruptions were observed in IGE-GTCS and the majority of aberrant functional connectivity manifested itself in default mode network. In addition, temporal metrics derived from state transition vectors were altered in patients including the total number of transitions across states and the mean dwell time, the fraction of time spent and the number of subjects in specific FNC state. Furthermore, the alterations were significantly correlated with disease duration and seizure frequency. It was also found that dynamic FNC could distinguish patients with IGE-GTCS from controls with an accuracy of 77.91% ($P < 0.001$). Taken together, this study not only provided novel insights into the pathophysiological mechanisms of IGE-GTCS but also

Contract grant sponsor: 863 project; Contract grant number: 2015AA020505; Contract grant sponsor: Natural Science Foundation of China; Contract grant numbers: 81501451, 61533006, 31600930, 11526149, and 61603272; Contract grant sponsor: Fundamental Research Funds for the Central Universities; Contract grant number: ZYGX2013Z004; Contract grant sponsor: Youth Fund Project of Tianjin Natural Science Foundation; Contract grant number: 16JCQNJC03900.

*Correspondence to: H. Chen, School of Life Science and Technology, University of Electronic Science and Technology of China, Chengdu 610054, People's Republic of China. E-mail: chenhf@uestc.edu.cn Or G. Lu, Department of Medical Imaging, Jinling Hospital, Nanjing 210002, People's Republic of China. E-mail: cjr.luguangming@vip.163.com

Received for publication 1 January 2016; Revised 27 September 2016; Accepted 28 September 2016.

DOI: 10.1002/hbm.23430
Published online 11 October 2016 in Wiley Online Library (wileyonlinelibrary.com)

suggested that the dynamic FNC analysis was a promising avenue to deepen our understanding of this disease. *Hum Brain Mapp 38:957–973, 2017.*

Key words: IGE-GTCS; resting-state fMRI; dynamic functional network connectivity; clustering and state analyses; default mode network

INTRODUCTION

Idiopathic generalized epilepsy (IGE), characterized by the widespread generalized spike-and-waves or polyspike-waves and undetectable focal anatomical brain abnormalities, encompasses a group of epileptic disorders [Sullivan and Dlugos, 2004]. Generalized tonic–clonic seizure (GTCS) is the most common subtype of IGE, and is the one that needs the most medical attention [Engel, 2001]. Patients with IGE-GTCS typically have the seizure symptoms of rigid stiffening of the limbs, violent muscle contractions of entire body, and loss of consciousness which may cause severe injury even death [Jallon and Latour, 2005; Marini et al., 2003]. Meanwhile, there are cognitive impairments between seizures, including memory, attention, and executive dysfunctions [Hommet et al., 2006]. Although considerable efforts have been made in the past decade, the pathophysiological mechanism of IGE-GTCS remains largely unclear.

Recent advance in neuroimaging techniques allows for exploration of the human brain in an efficient and non-invasive way. Resting-state fMRI has been suggested as a promising approach to study intrinsic functional properties [Barkhof et al., 2014; Guo et al., 2012; Kong et al., 2016; Li et al., 2014b; Liu et al., 2013]. Functional impairments in IGE-GTCS are thought to be associated with abnormal multiple interconnected brain systems rather than isolated areas. For instance, Song et al. [2011] found significantly decreased functional connectivity (FC) within the default mode network (DMN) of 14 IGE-GTCS patients compared with 29 healthy controls, suggesting that abnormal connectivity in the DMN might be the neural substrate of the impaired consciousness. In a dataset of 16 IGE-GTCS patients and 16 healthy subjects, Wang et al. [2011] observed disrupted FC in several resting-state networks (RSNs) such as the visual, auditory and dorsal attention networks, which might underlie the impairment of corresponding cognitive functions in the patients. However, these studies focused on the FC within single functional network with a relatively small sample size, and none of them examined between-network interactions in IGE-GTCS. The human brain is a complex, interconnected system with an optimal balance between functional specialization and integration. Exploration of the intra-network connectivity can enhance our understanding of the functional segregation, while investigation on the inter-network connectivity can advance our understanding of the functional integration of the brain. Therefore, examination of the FC between RSNs, namely functional network connectivity (FNC), may provide novel insights into the pathophysiological mechanism of IGE-GTCS.

Traditional FC analysis measures the correlations of signals within 5 minutes or more, with an assumption that the FC remains constant during the observation period [Biswal et al., 1995; Fox et al., 2005; Wang et al., 2016b]. Based on this hypothesis, one can obtain a static pattern of brain activity coherence, which is essentially an average connectivity over the whole period of time. Although static FC is widely used in previous literatures [Greicius, 2008; Liu et al., 2015a; Van den Heuvel and Hulshoff Pol, 2010], it may not be enough to fully characterize the human brain. The time-dependent and dynamic nature of brain activity reinforces the expectation that FC calculated on fMRI varies over time [Rabinovich et al., 2012; Sporns, 2011; Von der Malsburg et al., 2010]. Recently, a growing body of research has investigated the dynamic FC in healthy subjects and patients with neuropsychiatric diseases. For example, Allen and colleagues [Allen et al., 2014] examined resting-state FC dynamics in healthy young adults, and in a follow-up study, they found dynamic FC alterations in schizophrenia [Damaraju et al., 2014]. Shen et al. [2016] revealed the influence of driving behavior on the temporally dynamic properties of resting-sate FC. Liao et al. [2014] observed a complex transition of functional network topology as well as dynamic changes of connectivity between the thalamus and the DMN in absence epilepsy. These collective findings imply that dynamic FC is a promising avenue for clinical neuroimaging and can enrich our knowledge of functional organization of human brain [Calhoun et al., 2014; Kopell et al., 2014; Kucyi and Davis, 2015; Zhang et al., 2016].

Inspired by previous work, we compared the dynamic FNC in a relatively large sample of 50 IGE-GTCS patients with that in 50 age-, gender-, and handedness-matched healthy controls. Briefly, group independent component analysis (ICA) was first used to extract RSNs, and dynamic FNC matrices were then created using sliding window correlation approach. Subsequently, *K*-means algorithm was employed to cluster these matrices into different dynamic states, and state analysis was finally carried out to compare the dynamic FNC and temporal metrics between the two groups. Specifically, the optimal window size in the sliding window method was determined by a multivariate pattern analysis (MVPA). The aim of the current study was mainly twofold: we sought to explore whether IGE-GTCS had changed dynamic properties and, if so, whether those disease-related alterations were associated with clinical variables. Rather than focusing on

networks of interest which was commonly adopted in previous IGE-GTCS studies, in this work, we examined the whole-brain FC at the network level. This exploration was helpful in detecting potentially changed network interactions in IGE-GTCS, and may provide novel insights for extending the current knowledge of the neuropathological underpinnings of this disease.

MATERIALS AND METHODS

Participants

The present study was approved by the Ethics Committee of Jinling Hospital, Nanjing University School of Medicine. Written informed consent was obtained from each subject before any study procedure was initiated. Fifty patients with IGE-GTCS were recruited and they were all diagnosed as IGE with only GTCS based on the International League against Epilepsy (ILAE) classification: (1) presence of typical clinical symptoms of GTCS, including tic of limbs followed by a clonic phase of rhythmic jerking of the extremities, loss of consciousness during seizures and no partial seizures; (2) presence of generalized spike-and-wave or poly-spike-wave discharges in their interictal scalp electroencephalogram (EEG); (3) no focal abnormality in the structural MRI; and (4) no obvious history of etiology. In the current study, the patient's cohort included 11 drug-naive patients who were newly diagnosed as epilepsy, and the remaining 39 patients with IGE-GTCS were treated with antiepileptic drugs, including valproate, phenytoin, carbamazepine, lamotrigine, and topiramate. In addition, 50 age-, gender-, handedness-matched healthy controls were recruited. They were interviewed to confirm that none of them had a history of neurological or psychiatric disorder and no gross abnormalities. All the patients and controls were right-handed according to the criterion of Chinese revised-version of Edinburgh Handedness Inventory [Oldfield, 1971].

Data Acquisition

Scanning took place on a Siemens 3T Trio scanner (Siemens Medical Systems, Erlangen, Germany) with an eight-channel phased array head coil at Jinling Hospital, Nanjing, China. Foam padding was used to minimize head movement. During data acquisition, the participants were instructed to hold still, close eyes, relax minds and not to fall asleep (confirmed by all participants immediately after the experiment). Resting-state fMRI were acquired by a single-shot, gradient-recalled echo planar imaging (EPI) sequence. Sequence parameters were as follows: repetition time = 2,000 ms, echo time = 30 ms, slice thickness = 4 mm, slice gap = 0.4 mm, field of view = 24 cm, flip angle = 90°, in-plane matrix = 64 × 64, voxel size = 3.75 × 3.75 × 4 mm^3. For each subject, the brain volume comprised 30 axial slices, and each functional run contained 250 image volumes. During fMRI scan, no patient had seizure.

Overview of Methodology

An overview of the framework is summarized in Figure 1. First, resting-state fMRI data were preprocessed using SPM software (www.fil.ion.ucl.ac.uk/spm). Second, ICA was conducted at the group level to decompose the data into 34 independent components and then 21 RSNs were identified. Third, the optimal window length for calculating dynamic FNC was determined using an MVPA approach. Fourth, dynamic FNC matrices were calculated for each subject. Finally, clustering and state analyses were conducted to investigate the dynamic FNC changes in IGE-GTCS.

Data Preprocessing

Functional images were preprocessed using the SPM8 software package. After removing the first 10 images to allow the signal to reach equilibrium, fMRI data were corrected for the temporal differences between slices and head motion. Next, the corrected functional data were spatially normalized to the Montreal Neurological Institute EPI template in SPM8 using an optimum 12-parameter affine transformation and non-linear deformations and resampled to 3 × 3 × 3 mm^3. Finally, the normalized images were smoothed with an 8-mm full-width half maximum isotropic Gaussian kernel.

ICA

Group spatial ICA was adopted to decompose all preprocessed data into independent components (ICs) using GIFT software (version 2.0a [Calhoun et al., 2001]) with three steps: dimensionality reduction, ICs estimation, and back reconstruction. Specifically, a two-step principal component analysis was applied to reduce the data into 34 components, and the component number was determined by the minimum description length criterion [Li et al., 2007]. Subsequently, the Infomax algorithm [Bell and Sejnowski, 1995] was utilized in ICs estimation, which was run 100 times using the ICASSO algorithm to identify the most stable and reliable components [Himberg et al., 2004]. Next, a dual-regression method was employed to back-reconstruct the individual subject's components. After back-reconstruction, the ICs' time courses and spatial maps for all participants were obtained, and the subject-specific maps were converted to Z-scores (subtracting the mean and then dividing the result by the standard deviation). Here, all ICs were evaluated based on the group IC maps according to the following criteria [Beckmann et al., 2005; Cohn et al., 2015; Cordes et al., 2000; Damoiseaux et al., 2006; Zuo et al., 2010]: the RSNs exhibited peak activations in gray matter, had time courses dominated by low-frequency fluctuations (based on a frequency analysis

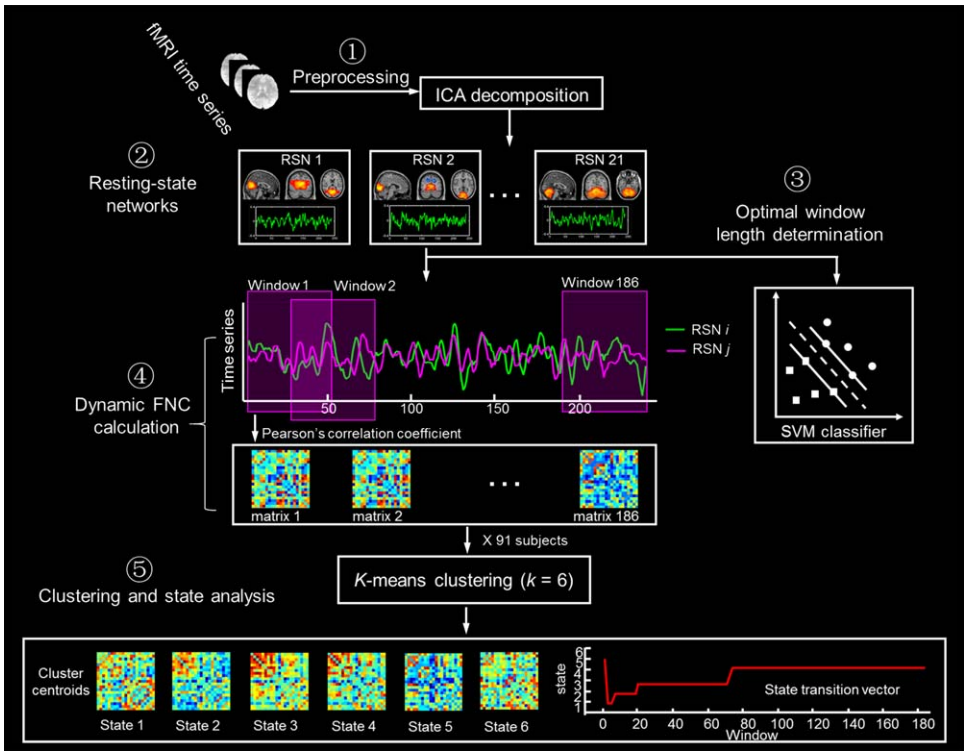

Figure 1.

An overview of analysis steps of dynamic functional network connectivity. The analysis includes the following steps: (1) resting-state fMRI data were preprocessed; (2) ICA was conducted and 21 RSNs were identified; (3) the optimal window length for calculating dynamic FNC was determined by an MVPA approach; (4) dynamic FNC matrices were calculated in all different sliding windows for each subject; (5) clustering and state analyses were conducted to investigate the dynamic FNC changes. Abbreviations: FNC, functional network connectivity; ICA, independent component analysis; RSN, resting-state network; SVM, support vector machine. [Color figure can be viewed at wileyonlinelibrary.com]

of the spectra of the estimated ICs), and showed low spatial overlap with known white matter structures, vascular, ventricles, motion and susceptibility artifacts. Finally, 21 functionally relevant RSNs were identified for the subsequent analyses.

Head Motion Correction

Recent studies have demonstrated that head motion has a substantial impact on resting-state FC [Power et al., 2014, 2015]. Although ICA can separate motion artifact from the selected RSNs [Kochiyama et al., 2005; Liao et al., 2006], we still used the following five steps to further minimize the effects of head motion. First, in the data preprocessing, we performed three-dimensional motion correction by aligning each functional volume to the mean image of all volumes, and excluded subjects whose head motion exceeded a translation of 2 mm or an angular rotation of 2 degrees in any direction. Second, we calculated the maximum motion between two successive images and discarded subjects with displacement more than 1 mm. Third, several summary metrics (mean, maximum, root mean square and mean frame-wise displacement) were estimated from the head motion profiles (3 translations and 3 rotations) in the remaining subjects. Statistical comparisons revealed that all these measures were matched between the two groups (all $Ps > 0.05$). Fourth, we regressed out head motion from the time courses of RSNs using Friston's 24-parameter model, as previously suggested [Friston et al., 1996; Yan et al., 2013]. Finally, an outlier detection strategy was utilized to find the affected time points using 3DDESPIKE (http://afni.nimh.nih.gov/afni) and the outliers were replaced with the best estimate using a third-order spline fit to the clean portions of the time courses [Allen et al., 2014].

Dynamic FNC Computation

Low frequency fluctuations of the resting-state fMRI signal were of physiological significance and thought to reflect spontaneous neural activity [Biswal et al., 1995; Lu et al., 2007]. Therefore, before dynamic FNC computation,

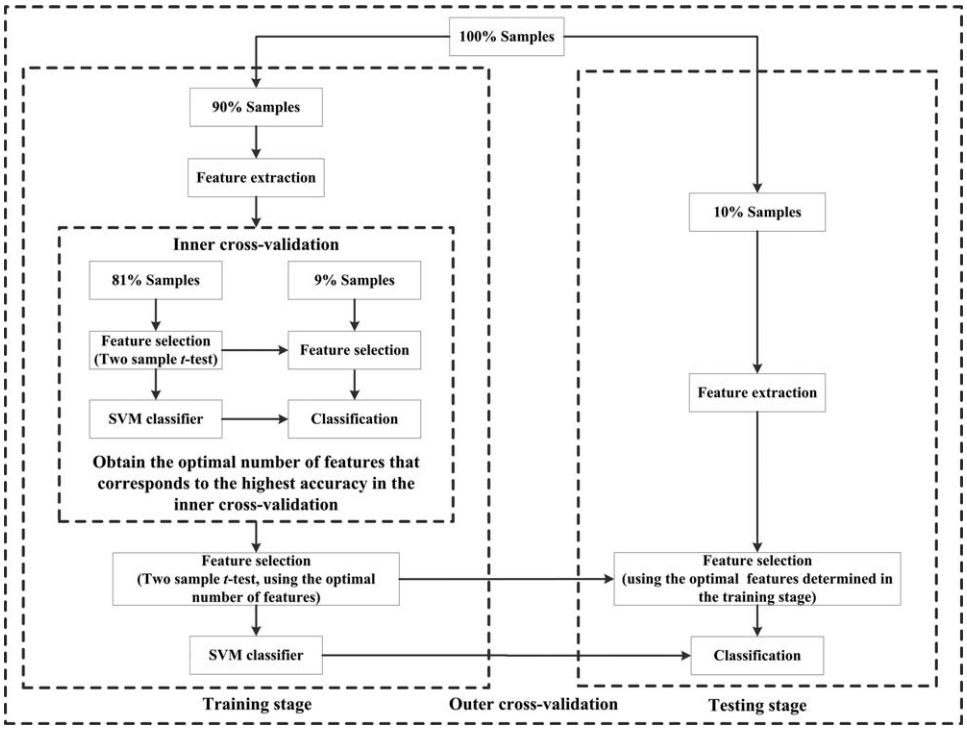

Figure 2.

Schematic overview of the nested 10-fold cross-validation classification framework. The inner cross-validation was used to determine the optimal number of features and the outer cross-validation was employed to estimate the classification performance. The whole nested cross-validation process was repeated 10 times, and the final result was the average accuracy of 10 repetitions of 10-fold cross-validation.

the time courses of RSNs were temporally bandpass filtered (0.01–0.08 Hz) to reduce the effects of low-frequency drift and high-frequency physiological noise [Liu et al., 2012c].

The dynamic FNC was computed using a sliding window correlation approach. Since there was currently no formal consensus regarding the window length, we selected a range of length (10–75 TRs, step = 1 TR) according to former studies [Hutchison and Morton, 2015; Leonardi and Van De Ville, 2015; Liao et al., 2014; Zalesky and Breakspear, 2015]. The optimal window length (55 TRs) was determined by using MVPA (see details in the **IGE-GTCS Classification** section below) and the window was shifted with a step size of 1 TR (i.e., 2 s) each time, resulting in 186 windows in total. In each window, the time courses of each pair of the 21 RSNs were used to calculate FNC (Pearson's correlation coefficient) and a 21 × 21 correlation matrix was obtained. A Fisher's r-to-z transformation [Cohen et al., 2013; Liu et al., 2015b] was then applied to all FNC matrices to improve the normality of the correlation distribution as

$$z = \frac{1}{2}[\ln(1+r) - \ln(1-r)] \quad (1)$$

where r is the Pearson correlation coefficient and z is approximately a normal distribution.

IGE-GTCS Classification

For a given window length, we calculated temporal variabilities of connections between RSNs over time and considered them as features for classifying IGE-GTCS from healthy controls. The variance of the time series of correlation coefficient was computed to assess temporal variability according to the equation:

$$Var_{DFNC(i,j)} = \frac{1}{N-1}\sum_{n=1}^{N}\left(z_n(i,j) - \frac{1}{N}\sum_{n=1}^{N} z_n(i,j)\right)^2 \quad (2)$$

where $z_n(i,j)$ was the FNC strength between RSN i and RSN j within a given sliding window n, and N was the total number of windows. Thus, for each subject, a 21 × 21 variance matrix was finally obtained, resulting in $(21 \times (21-1))/2 = 210$ classification features.

Given that some features are non-informative or redundant for classification, feature selection was adopted to improve classification performance and to speed up

computation. As did in previous studies [Cui et al., 2016; Zeng et al., 2012], a univariate feature-filtering method was employed here. Specifically, two-sample two-tailed *t*-tests were performed on the features in the training set to determine the features that showed differences between the IGE-GTCS and control groups, and then the features were ranked according to their *P* values (in the ascending order). The first *M* ranking features, which corresponded to the *M*-smallest *P* values, were retained and the remaining ones were discarded. A nested 10-fold cross-validation strategy was applied here [Liu et al., 2014; Thung et al., 2014; Zhu et al., 2014], with the outer cross-validation to estimate the classification performance and the inner cross-validation to determine the optimal *M*. In brief, all samples were randomly partitioned into 10 subsets. Among them, nine subsets were selected for training and the remaining one was utilized for testing. During the training procedure, 210 inner 10-fold cross-validations, with each one corresponding to a different *M* threshold (1–210), were applied. Once we got the highest classification accuracy in the inner cross-validation with the first *M* features, we defined *M* as the optimal number of features. This threshold (*M*-first) was adopted in the training set of the outer cross-validation for the final classification. The whole nested cross-validation procedure was repeated 10 times to avoid any bias introduced by random partitioning in the cross-validation. Result reported was the average accuracy of 10 repetitions of 10-fold cross-validation. A linear support vector machine (SVM) classifier was employed to discriminate IGE-GTCS from healthy controls, which was implemented using LIBLINEAR toolbox [Fan et al., 2008], with a default value for the parameter *C* (i.e., $C = 1$). Finally, we obtained classification accuracy for each window length, and the optimal length corresponded to the peak accuracy.

Permutation test was performed to determine whether the peak classification accuracy exceeded chance level [Liu et al., 2012b; Zeng et al., 2012]. To achieve this aim, the class labels were permuted 10,000 times (randomly reallocating patient and control labels to the training subjects) and repeated for the entire classification processes. We counted the number of times when the accuracy was greater than the one obtained by the real labels. After dividing by the total number of permutations, the *P* value was obtained. The schematic overview for the whole classification framework is shown in Figure 2.

Clustering Analysis

We adopted *k*-means algorithm to cluster all dynamic FNC matrices to assess the frequency and structure of reoccurring FNC connectivity patterns. The L_1 (Manhattan) distance was used as a similarity measure in clustering, as it was suggested by Aggarwal et al. [2001] that L_1 was more effective in measuring the similarity of high-dimensional data. Moreover, a subsampling analysis was conducted within each subject along the time dimension to reduce the computational demands and to diminish redundancy between windows. Briefly, guided by previous studies [Allen et al., 2014; Shen et al., 2016], we first selected subject exemplars as those windows with local maxima in FC variance. Second, *k*-means clustering was performed to all exemplars and repeated 500 times with random initial cluster centroid positions to escape local minima. The optimal number of clusters was estimated using the elbow criterion, calculating as the ratio of within-cluster distance to between-cluster distance. A *k* of 6 was determined in a search window of *k* ranging from 2 to 20. Finally, the resulting cluster centroids were used as starting points to cluster all data (91 subjects $\times$ 186 windows = 16,926 matrices) into 6 clusters, and the cluster medians were regarded as FC states.

State Analysis

We compared the subject medians of each state between the two groups using a network-based statistic (NBS) approach. This method assumes that the disrupted connections are interconnected into a subnetwork which is more likely to indicate real alterations than isolated dysconnections, and has been shown to yield substantially greater statistical power than generic methods to control the family-wise error [Zalesky et al., 2010]. In brief, a primary cluster-forming threshold ($P < 0.01$, uncorrected) was first used to identify a set of supra-threshold connections, within which any connected components and their size (number of connections) could then be determined. A corrected *P* value was computed for each component using the null distribution of maximal connected component size, which was obtained using a nonparametric permutation approach (10,000 permutations). For details of the NBS method, see the study by Zalesky et al. [2010].

In addition, we performed an exploratory experiment in which we calculated and compared temporal metrics derived from each subject's state vector [Allen et al., 2014]. Specifically, we computed four measures in each subject, including: (1) mean dwell time in each state, measured as the average number of consecutive windows in the same state; (2) fraction of time spent in each state, measured as the proportion of all windows in each state; (3) total number of transitions, measured as the number of state transitions; and (4) mean state transition probability, measured as the probability of transitioning from one state to another state. Permutation tests were utilized to evaluate between-group differences of these metrics [Liu et al., 2016; Wang et al., 2013]. To this end, we first computed the real between-group difference in the mean value of each measure, and then randomly reassigned all the values of this measure into the two groups for 10,000 times and recalculated the mean difference between these two randomized groups. If less than 5% of the randomized between-group differences were equal or greater than the non-permutated value, the result was regarded significant. Finally, we counted FC states at the group level as the

TABLE I. Characteristics of the patients with IGE-GTCS and healthy controls

Variables (Mean ± SD)	IGE-GTCS	HC	*P* value
Gender (M/F)	43 (28/15)	48 (29/19)	0.644
Age (years)	23.12 ± 4.80	23.02 ± 1.49	0.896
Handedness (right/left)	43/0	48/0	–
Duration (years)	6.48 ± 5.80	–	–
Onset age (years)	16.77 ± 5.03	–	–
Frequency (times/year)	26.04 ± 77.96	–	–

The *P* values were obtained by a two-sample *t*-test for age, and a chi-square test for gender. Abbreviations: F, female; GTCS, generalized tonic-clonic seizure; HC, healthy controls; IGE, idiopathic generalized epilepsy; M, male; SD, standard deviation.

number of subjects in each state, and compared them using the proportion tests.

Correlation Analysis

Once significant between-group differences were found in any dynamic measures, the relationships between these measures and clinical variables (i.e., illness duration, onset age, and seizure frequency) were assessed in the patient group using Spearman's rank correlation coefficient. The threshold of $P < 0.05$ was considered to be significant for these analyses.

Control Analysis

To further validate our findings, we performed the following four experiments.

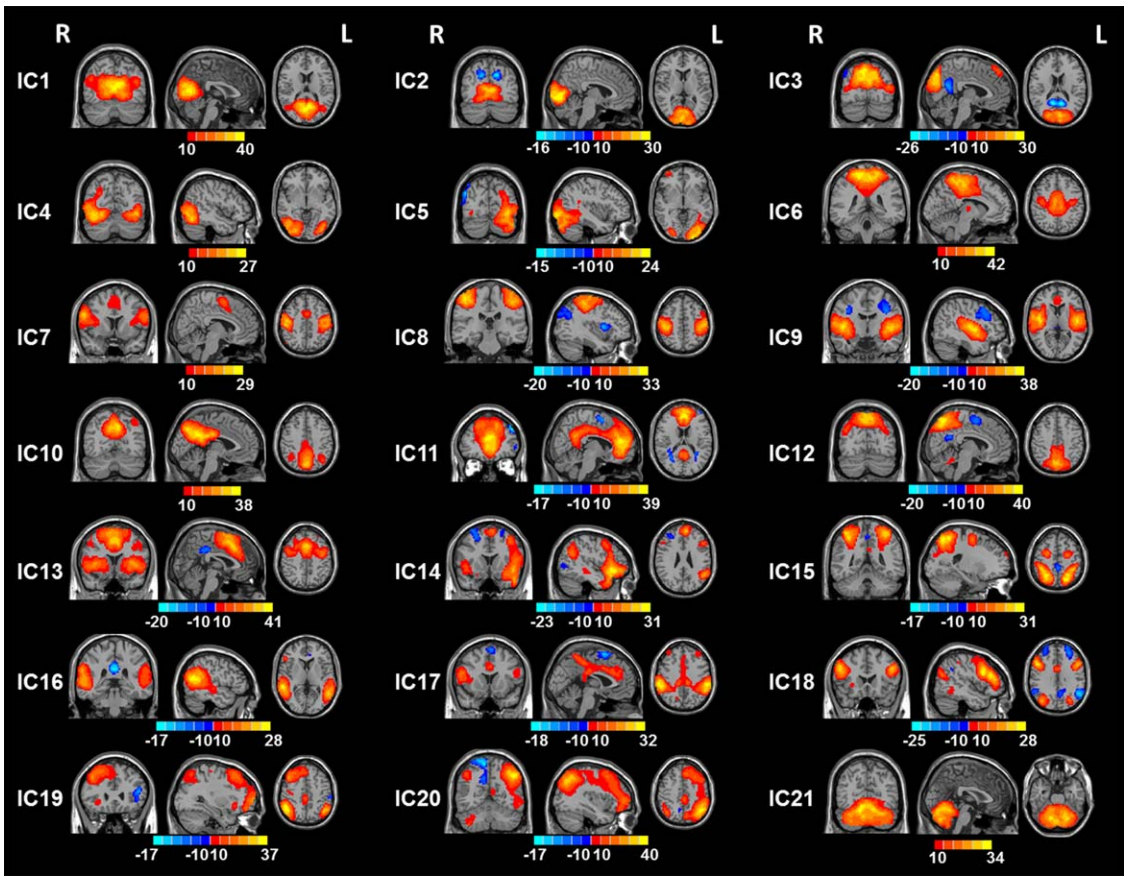

Figure 3.

The 21 functionally relevant RSNs. The spatial maps of all subjects of each RSN were entered into a random-effect one-sample *t*-test, and we used a threshold of $|t| > 10$ to select voxels of a component to improve the representativeness of each RSN. Based on the anatomical and functional properties of ICs, ICs 1-5, ICs 6-8, IC 9, ICs 10-11, ICs 12-20, and IC 21 were categorized into the VN, SMN, AN, DMN, CCN, and CER, respectively. The color bar represents *t* values. Abbreviations: IC, independent component; L, left; R, right. [Color figure can be viewed at wileyonlinelibrary.com]

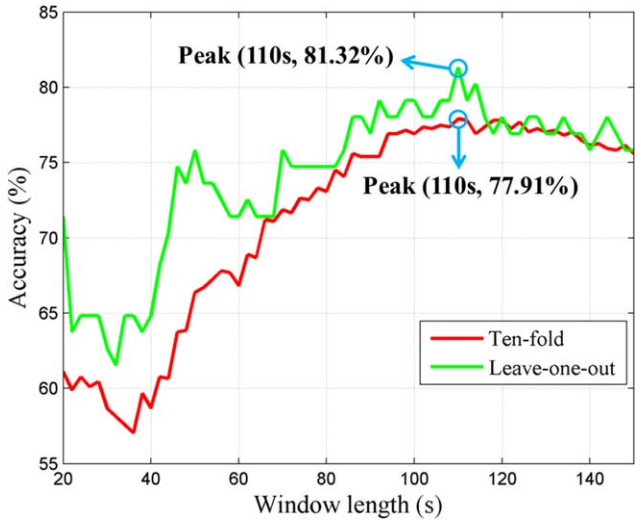

Figure 4.

Classification accuracy as a function of the window length obtained by nested 10-fold (red line) and leave-one-out (green line) cross-validation. Blue circles represent the peak accuracies. [Color figure can be viewed at wileyonlinelibrary.com]

First, we performed a nested leave-one-out cross-validation (LOOCV) on our data to estimate the classification performance. Although LOOCV may introduce a high degree of variance in testing on a single subject per fold, this strategy was almost unbiased [Efron, 1983] and was widely used in the previous epilepsy studies [Fang et al., 2015; Focke et al., 2012; Zhang et al., 2012].

Second, the MVPA was used to classify the patients with IGE-GTCS from healthy controls in the current study. This technique takes into account classification features jointly, and thus makes full use of the complementary information among features. To validate this advantage, we calculated the accuracy using the same nested 10-fold cross-validation based on each of the 210 dynamic features and compared it with MVPA. Specifically, the outer cross-validation was applied to estimate the classification performance and the inner cross-validation was adopted to determine the optimal cut-off value for separating two groups.

Third, the static FNC was obtained by computing temporal correlation of whole time courses (no sliding window) of each pair of the 21 RSNs. After Fisher's r-to-z transformation, the same classification procedures (including feature selection and cross-validation) were performed

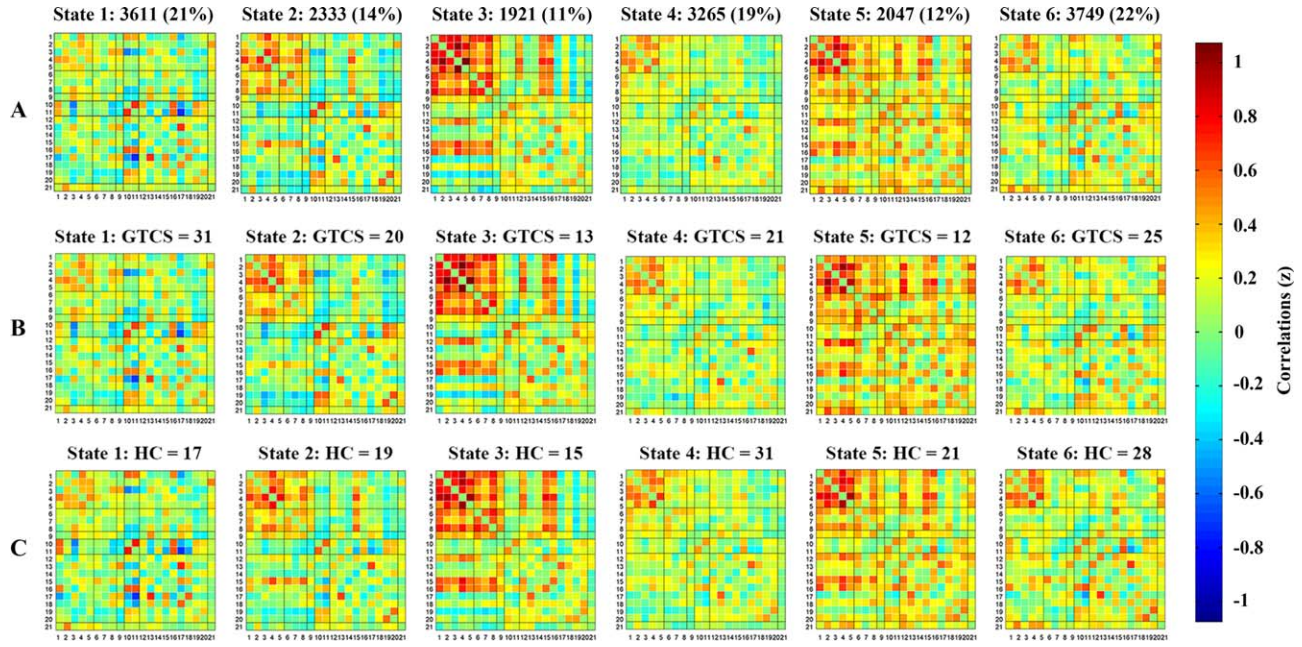

Figure 5.

The six cluster medians of all subjects are shown in (A) along with the total number and the percentage of occurrences. Group specific centroids of the states for patients with IGE-GTCS and healthy controls together with the count of subjects that had at least one window in each state are shown in (B) and (C), respectively. The color bar represents z value of FNC. Abbreviations: GTCS, generalized tonic-clonic seizure; HC, healthy controls. [Color figure can be viewed at wileyonlinelibrary.com]

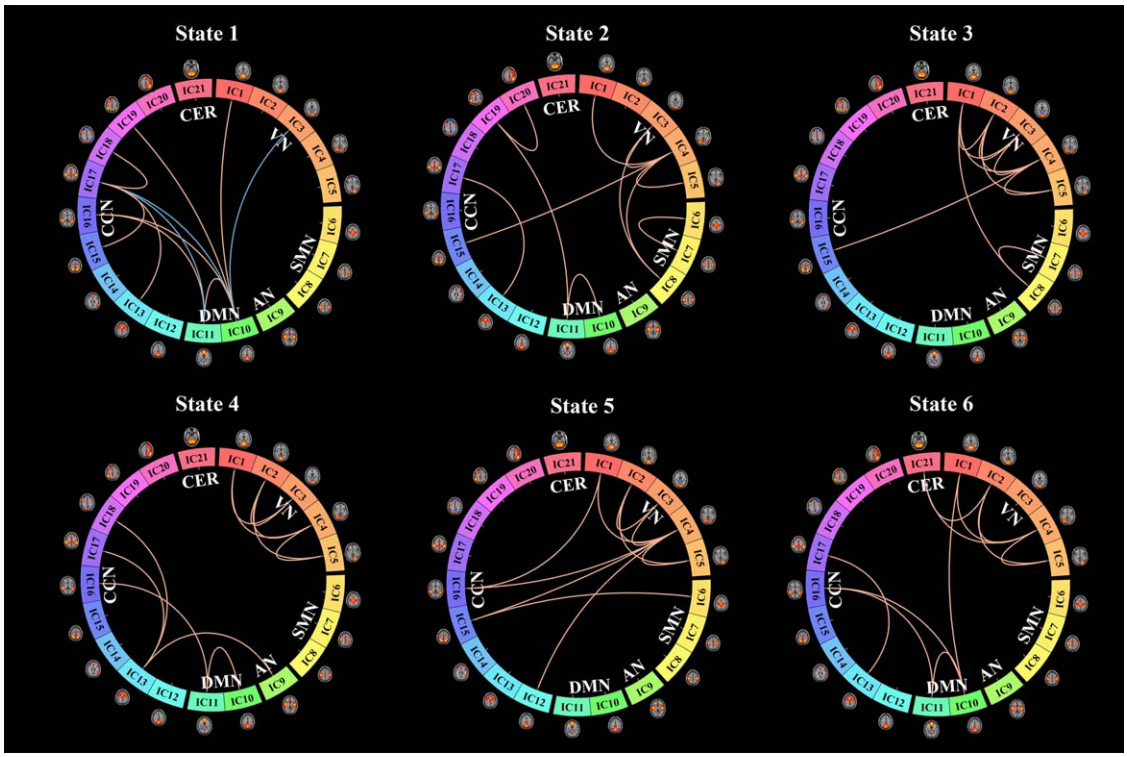

Figure 6.

The strongest 5% connections of each state. Each rectangle on the circumference of the big circle represents each IC, and the gaps between the rectangles separate different functional subsystems (i.e., VN, SMN, AN, DMN, CCN, and CER). The lines connecting the rectangle pairs represent the connections between the corresponding two ICs. The red lines represent positive connections and blue lines denote negative connections. Based on the anatomical and functional properties of ICs, ICs 1-5, ICs 6-8, IC 9, ICs 10-11, ICs 12-20, and IC 21 were categorized into the VN, SMN, AN, DMN, CCN, and CER, respectively. Abbreviation: IC, independent component; VN, visual network; SMN, sensorimotor network; AN, auditory network; DMN, default mode network; CCN, cognitive control network; CER, cerebellum. [Color figure can be viewed at wileyonlinelibrary.com]

to investigate the diagnostic value of static FNC. Moreover, we compared the static FNC differences between the two groups using the NBS method.

Finally, the temporal variabilities (i.e., classification features) of connections between RSNs were compared between the two groups. Outcomes were examined at two commonly used statistical thresholds: corrected for multiple comparisons using (1) a Bonferroni correction of $P < 0.05$, and (2) a false discovery rate correction of $P < 0.05$.

RESULTS

Demographics and Clinical Characteristics of the Participants

One patient was excluded because head motion exceeded a translation of 2 mm or an angular rotation of 2 degrees, and six patients and two healthy controls were discarded due to the maximum displacement between two successive images larger than 1 mm. The remaining subjects included 43 IGE-GTCS patients and 48 healthy controls. Chi-square test was performed to evaluate the differences in gender, and two-sample *t*-test was performed to evaluate the differences in age. The results revealed that the two groups were matched for gender (28 males for the IGE-GTCS and 29 males for the control group; $P = 0.644$), handedness (all the subjects in two groups are right-handed) and age (23.12 ± 4.80 years for the IGE-GTCS and 23.02 ± 1.49 years for the healthy controls; $P = 0.896$). In addition, the illness duration, onset age and seizure frequency were 6.48 ± 5.80 years, 16.77 ± 5.03 years and 26.04 ± 77.96 times per year of the patients, respectively. The detailed demographic and clinical data are shown in Table I.

Resting-State Networks

A total of 34 ICs were obtained by ICA and 21 ICs were identified as RSNs (Fig. 3). Based on their anatomical and

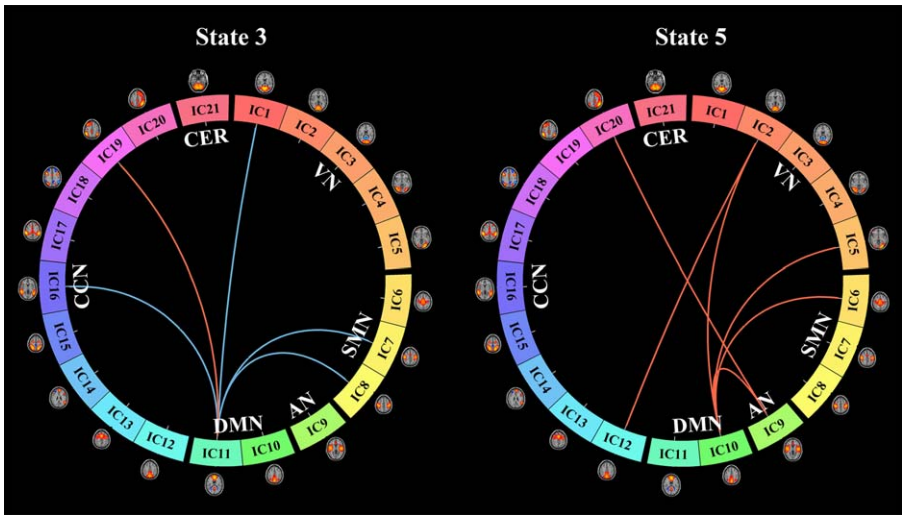

Figure 7.

Significant between-group FNC differences. Each rectangle on the circumference of the big circle represents each IC, and the gaps between the rectangles separate different functional subsystems (i.e., VN, SMN, AN, DMN, CCN, and CER). The lines connecting the rectangle pairs represent the connections between the corresponding two ICs. The red lines represent significantly increased connections and the blue lines denote significantly decreased connections in IGE-GTCS. Based on the anatomical and functional properties of ICs, ICs 1-5, ICs 6-8, IC 9, ICs 10-11, ICs 12-20, and IC 21 were categorized into the VN, SMN, AN, DMN, CCN, and CER, respectively. Abbreviations: IC, independent component. VN, visual network; SMN, sensorimotor network; AN, auditory network; DMN, default mode network; CCN, cognitive control network; CER, cerebellum. [Color figure can be viewed at wileyonlinelibrary.com]

functional properties, ICs 1-5, ICs 6-8, IC 9, ICs 10-11, ICs 12-20, and IC 21 were grouped into the visual network (VN), sensorimotor network (SMN), auditory network (AN), default mode network (DMN), cognitive control network (CCN), and cerebellum (CER), respectively. This parcellation was in line with former studies [Allen et al., 2014; Rashid et al., 2014]. The remaining 13 non-RSN ICs are shown in Supporting Information Figure S1.

Classification Results

As shown in Figure 4, the accuracy of linear SVM classifier could reach up to 77.91% ($P < 0.001$) with the window size of 110s (55 TRs) via a nested 10-fold cross-validation. In addition, the mean variance of accuracy over folds was 3.87×10^{-4}.

Clustering Analysis

As mentioned above, we utilized *k*-means approach to cluster the dynamic FNC matrices from all subjects. Each matrix in Figure 5A, which is arranged in the order of emergence, represents cluster centroid and reflects the FC state within the data. Differences among these matrices are apparent in the sign and the magnitude of connectivity between RSNs. Here, we delineated the distinctions of different states in terms of strong connections, although additional differences were also present. For better visualization, we kept the strongest 5% connections of each state to clearly show the divergent pattern among FC states (Fig. 6). Basically, the cerebral RSNs could be divided into two categories, the low-level perceptual network (VN, SMN, and AN) and the high-level cognitive network (DMN and CCN). In state 1, the strong connections were mainly found in cognitive network, particularly within DMN/CCN and between these two networks. State 2 exhibited distributed strong connections between RSNs. Although states 3–6 shared the similarity that strong correlations mainly concentrated within perceptual networks (particularly VN), they still possessed some unique connection patterns. In state 3, almost all the connections were within perceptual network. State 4 showed high correlation within perceptual and cognitive networks. In addition to the within-perceptual network connections, state 5 had several connections between perceptual and cognitive networks. State 6 was similar to state 4 except for the connectivity between DMN and VN.

State Analysis

The group-specific medians for each state are shown in Figure 5B,C. Of note, in consistent with previous dynamic

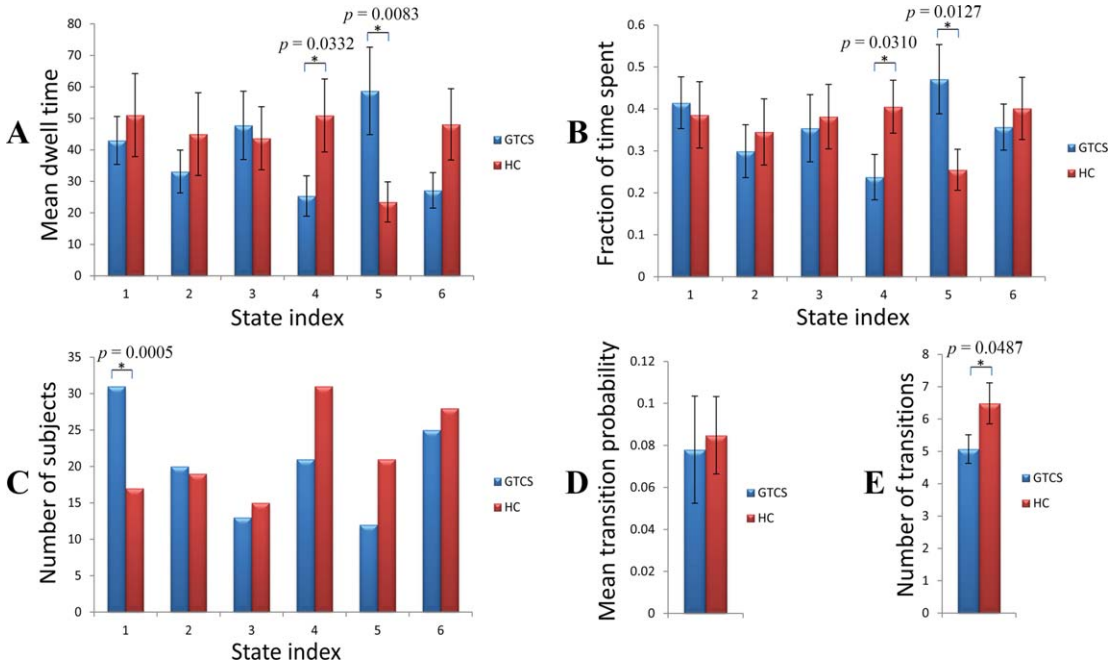

Figure 8.

Between-group comparison in temporal metrics derived from state transition vector. The black stars in bar plots denote statistically significant differences between the two groups. Error bars represent the standard error. Abbreviations: GTCS, generalized tonic-clonic seizure; HC, healthy controls. [Color figure can be viewed at wileyonlinelibrary.com]

FC studies [Allen et al., 2014; Damaraju et al., 2014; Shen et al., 2016], not all subjects had the windows assigned to each state (examples of state transition vectors are shown in Supporting Information Fig. S2), and thus the number of subject-specific matrices changed in different states (see subject counts per state shown in Fig. 8C). By using the NBS method, the group differences were found in state 3 ($P = 0.0345$) and state 5 ($P = 0.0149$), after family-wise error correction for multiple comparison (Fig. 7). We found significantly decreased connections between DMN and VN/SMN, and both increased and decreased connections between DMN and CCN in state 3. However, only significantly increased connections were found between DMN and VN, SMN and AN, between CCN and AN/VN in state 5. There was no significant alteration of FNC in other states.

We also found that, compared with healthy controls, IGE-GTCS patients had significantly shorter mean dwell time and fraction of time spent in state 4, while in state 5 they had significantly longer mean dwell time and fraction of time spent than healthy controls (Fig. 8A,B). With regard to the FC state counts for the two groups, the number of subject in state 1 in patient was significantly more than that of control group (Fig. 8C). In addition, there was significant difference in the number of transitions (Fig. 8E) but unchanged mean transition probability (Fig. 8D) between the two groups.

Correlation Analysis

We found that the connectivity between IC 1 and IC 11 in state 3 was negatively correlated with illness duration ($P = 0.005$), and the connectivity between IC 9 and IC 10 in state 5 was positively correlated with seizure frequency ($P = 0.045$). Additionally, the mean dwell time in state 4 was negatively correlated with seizure frequency ($P = 0.039$) and the total number of transitions was negatively correlated with illness duration ($P = 0.020$).

Control Analysis

As shown in Figure 4, the highest classification accuracy obtained by the nested LOOCV was 81.32% with the window length of 110s. In addition, based on single classification feature, the highest accuracy was 67.02%. With regard to static FNC, the linear SVM classifier obtained an average accuracy of 73.52%, and no significant difference was observed using the NBS method. Paired *t*-tests revealed that the accuracy obtained by dynamic features (77.91%)

was significantly higher ($P < 0.001$) than that achieved by single dynamic feature (67.02%) and static features (73.52%). Furthermore, no significant difference was found in temporal variabilities (i.e., classification features) between the two groups.

DISCUSSION

This is the first study, to our knowledge, to investigate dynamic FNC in a relatively large sample of IGE-GTCS. Our work revealed the following findings: (1) state-specific disrupted network interactions between RSNs were found in the patients and the pronounced abnormalities were mainly associated with DMN; (2) changed dynamic measures derived from state transition vector were observed in the patients including mean dwell time, fraction of time spent, number of subjects in some certain states and total number of transitions across states; (3) significant correlations between altered dynamic metrics and clinical characteristics were seen in the patients; and (4) a significantly high accuracy was achieved for IGE-GTCS classification by the dynamic FNC. These results provided evidence of the dynamic FNC alterations in the IGE-GTCS, which shed new light on the pathophysiological mechanisms underlying this disease.

In the past few years, investigating the functional interactions between RSNs has become a powerful tool to explore the human brain and holds great potential as a possible diagnostic avenue for neuropsychiatric disease [Jafri et al., 2008; Li et al., 2015; Wang et al., 2015; Zhang et al., 2015]. Such investigations were commonly derived from an fMRI experiment spanning from 5 to 10 minutes and based on an implicit assumption that FC was static over this period of time. However, this assumption was challenged in studies focused on time frequency analysis [Chang and Glover, 2010] and time-varying multivariate connectivity patterns [Sakoglu et al., 2010]. Since then, several dynamic FC studies have appeared to capture time-varying properties of connectivity (for a comprehensive review, see Hutchison et al., [2013a]). Two recent studies demonstrated the relationship between spontaneous brain dynamics and structural connectivity, providing the physical substrate of the temporal variability of FC [Liao et al., 2015; Shen et al., 2015].

As shown in Figure 7, significant between-group FNC differences were observed among several RSNs including DMN, CCN, VN, SMN and AN in state 3/state 5. The CCN primarily comprises fronto-parietal regions and is involved in top-down modulation of attention and working-memory tasks [Cole and Schneider, 2007]; the VN, SMN, and AN are involved in sensory perception and motor process which are responsible for information communication with external environment. The goal-directed decisions influence our perception and lead to corresponding modulation of sensory cortical activity, which is actually the top-down control and allows us to flexibly navigate

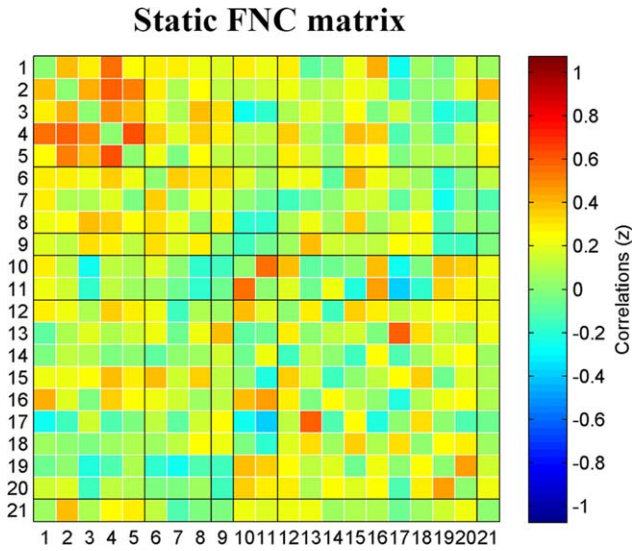

Figure 9.
Group mean static FNC map. The color bar represents z value of FNC. Abbreviations: FNC, functional network connectivity. [Color figure can be viewed at wileyonlinelibrary.com]

multiple streams of sensory information [Gazzaley et al., 2005a,b]. Therefore, the absence of functional connection between CCN and perceptual network, together with the impairment of perception observed in epilepsy in previous studies [Grant, 2005; Luo et al., 2011; Zhang et al., 2009], suggested the deficits of the high-order control over sensory process in IGE-GTCS.

It was worth noting that the disrupted FNCs were mainly related to DMN, which was active during resting state and inhibited in a wide range of cognitive tasks [Buckner et al., 2008; Raichle, 2015; Raichle et al., 2001]. Convergent evidence from functional brain imaging demonstrated high spatial overlap of functional hubs with regions of the DMN, indicating a critical role of the DMN in the overall network structure [Liu et al., 2015c; Tomasi and Volkow, 2011; Van den Heuvel and Sporns, 2013]. Furthermore, the DMN is one of the most important RSNs since it integrates information from primary function and cognition networks [Liao et al., 2010]. Recent literatures indicated that DMN had made it possible to distinguish IGE-GTCS from healthy controls, and both increased and decreased FC were observed in the DMN in IGE [McGill et al., 2012; Song et al., 2011; Wang et al., 2011]. The functional abnormality in DMN may influence its information communication with other networks, resulting in impaired functional integrations between the DMN and other RSNs. Intriguingly, the majority of pronounced changes in state 3 were hyperconnectivities and related to anterior DMN. In contrast, all significant alterations in state 5 were hypoconnectivities and associated with posterior DMN. A prior study showed a dissociation pattern in DMN that increased intra-network FC in posterior DMN was accompanied by

decreased intra-network FC in anterior DMN [Wang et al., 2011], which might provide a possible explanation of this result. These findings together with the relationships between altered FNC and clinical variables provided crucial information for better understanding of IGE-GTCS.

Significantly different connections were found in dynamic FNC but not in static FNC analysis. The reasons for this might be twofold: first, the connectivity pattern of state 4 was much similar to the pattern of static FNC (Fig. 9) based on the spatial correlation between static FNC matrix and the cluster centroid of each state. Thus, no significant FNC difference in state 4 might result in nonremarkable changes in static FNC; and second, static analysis actually represents a measure of average connectivity across different dynamic states by calculating FNC within the whole scanning period. Hence, it may not be sensitive enough to detect the between-group alteration. These two reasons highlighted the necessity of conducting dynamic FNC analysis, and our findings demonstrated that dynamic FNC could yield important information which could not be captured by static FNC. In this study, we also carried out the exploratory analysis of examining dynamic metrics derived from state vectors. Compared with healthy controls, patients dwelled for shorter duration and spent less time in state 4, but stayed longer and spent more time in state 5. Moreover, the total number of state transitions in patients was less than that of controls, and the number of subjects who had state 1 was more than that of controls. From the correlation analyses between these changed metrics and clinical variables, we found negative correlations between the number of transitions and illness duration, and between the mean dwell time in state 4 and seizure frequency, suggesting that these dynamic measures could be alternative indices for investigation on IGE-GTCS.

In the sliding window based dynamic FC analysis, window length is an open area of research and an important parameter to capture the resting-state FC dynamics. The window length should be short enough to permit the detection of non-stationary fluctuations and long enough to allow robust estimation of FC. In previous studies, the window length typically ranged from 12.5 to 240 s [Chang and Glover, 2010; Hutchison et al., 2013b; Kiviniemi et al., 2011; Liao et al., 2014; Shakil et al., 2016; Shen et al., 2016]. Recently, Leonardi and Van De Ville [2015] demonstrated that the minimum window length should be no less than $1/f_{\min}$, where $f_{\min}$ was the minimum frequency of the correlating time courses. The window size less than $1/f_{\min}$ would introduce spurious fluctuations. In the current study, a bandpass filter (0.01–0.08 Hz) was applied to minimize the effects of low-frequency drift and high-frequency physiological noises. The MVPA was utilized to determine the optimal and objective window size of 110 s, which was more accurate than other size for discriminating IGE-GTCS from healthy controls. This disease-specific window length (110 s) met the criterion of being greater than $1/f_{\min}$ ($1/0.01 = 100$ s), demonstrating the reasonability of the used window size. In addition, classification accuracies of 77.91% and 81.32% were obtained using nested 10-fold cross-validation and LOOCV, respectively. Both of these two results were obtained with the same window length of 110 s (Fig. 4), indicating the robustness of the used window length.

Although the classification result was not the main focus of this study (to determine the optimal window length), we compared the results with previous epileptic classification researches based on FC. Zhang et al. [2012] constructed FC matrix based on automated anatomical labeling template [Tzourio-Mazoyer et al., 2002] in mixed epileptic patients (including focal, generalized, and temporal lobe epilepsy), and achieved a cross-validated classification accuracy of 83.9%. Su et al. [2015] used predefined 160 regions of interest to create FC matrix in mesial temporal lobe epilepsy and obtained an accuracy above 90%. However, both of them utilized LOOCV to estimate the classification performance, which had a high variance in prediction error [Kohavi, 1995]. Moreover, they did not adopt a nested manner in cross-validation but directly constructed a model on the training data and tested on the test data in each cross-validation fold. Such procedures resulted in increased optimism because models were selected after peeking at the test results [Gabrieli et al., 2015]. To avoid this problem, one can choose models from cross-validation on the training data. In the present study, a nested cross-validation strategy was employed and a relatively high accuracy was obtained, providing evidence that IGE-GTCS could be classified from healthy controls at the individual level.

Compared with univariate analysis, MVPA considers the features jointly and makes full use of complementary information among features [Li et al., 2014a; Liu et al., 2012a; Shi et al., 2016; Wang et al., 2016a; Zeng et al., 2014]. Moreover, MVPA is sensitive to the fine-grained spatial patterns and subtle differences that would be undetectable using univariate method which focuses on gross differences at group level. In this work, we performed group comparison on classification features (temporal variabilities), but no significant difference was found after Bonferroni or false discovery rate correction, demonstrating that MVPA could still provide above chance-level classification even in the range of statistically non-significant univariate findings. We also acquired classification accuracy based on each of the 210 features and the highest accuracy was 67.02%. Furthermore, to compare the classification results between dynamic and static FNCs, the whole time courses of all 21 RSNs were used to compute temporal correlations. Classification accuracy was 73.52% when using static FNC features. These accuracies were significantly lower than our result (77.91%), demonstrating the superiority of dynamic FNC analysis in IGE-GTCS.

Several limitations of this study should be noted. The first is the fact that most IGE-GTCS patients are medicated.

Thus, our findings might be confounded by the use of antiepileptic drugs, which can affect the normal neuronal function and produce cognitive impairment [Loring and Meador, 2004]. Future studies need to be conducted to clarify this effect of antiepileptic drugs on dynamic FNC. Second, the fMRI data were acquired without simultaneous EEG. It is challenging to acquire fMRI of acceptable quality during the ictal state because of body movements. Therefore, the potential effects on dynamic FNC of interictal epileptiform activity could not be evaluated. Third, head motion has a confounding effect on resting-state FC. To alleviate this influence, we performed a series of procedures such as the use of motion regressors in the models, motion-related data exclusion criteria, between-group comparison of head motion profiles, and outlier detection strategy. However, the head motion effect may not be fully ruled out. Fourth, we did not use MVPA to explore the between-group difference in the state analysis because the changing number of subject-specific matrices in each state would lead to different number of classification features in each subject. In the future, it would be interesting to develop new MVPA methods to conduct such analysis. Fifth, we did not evaluate the influence of the temporal dependence of overlapping windows on MVPA which would be tested in separate studies in the future. Sixth, despite the fact that between-group differences were found in temporal metrics, the neurobiological meaning behind these alterations is not clear yet and should be elucidated in future studies. Finally, although the cross-validation approach was employed to evaluate the classification performance, independent dataset is needed to confirm our results in the future.

CONCLUSION

In summary, this study represented the first attempt to examine dynamic FNC among whole-brain RSNs in IGE-GTCS. The main findings were that the aberrant FNC patterns were state-dependent, and the altered connectivity was mostly concentrated in the DMN. In addition, the changes of dynamic metrics derived from state transition vector were also observed. Some of these alterations were found to be correlated with clinical variables, which may ultimately contribute to the identification of neuroimaging based biomarkers and the potential aid in early intervention in IGE-GTCS. Overall, these findings provided a novel perspective on the pathophysiology mechanisms of IGE-GTCS, and implicated new directions for future research by means of dynamic FNC to investigate other types of epilepsy.

ACKNOWLEDGMENTS

We thank the three anonymous reviewers for their constructive suggestions. We also thank Yali Jiang, Yanjun Li, and Junping Wang for the valuable feedback on this work.

REFERENCES

Aggarwal CC, Hinneburg A, Keim DA (2001): On the Surprising Behavior of Distance Metrics in High Dimensional Space. New York: Springer.

Allen EA, Damaraju E, Plis SM, Erhardt EB, Eichele T, Calhoun VD (2014): Tracking whole-brain connectivity dynamics in the resting state. Cereb Cortex 24:663–676.

Barkhof F, Haller S, Rombouts SA (2014): Resting-state functional MR imaging: A new window to the brain. Radiology 272: 29–49.

Beckmann CF, DeLuca M, Devlin JT, Smith SM (2005): Investigations into resting-state connectivity using independent component analysis. Philos Trans R Soc Lond B Biol Sci 360: 1001–1013.

Bell AJ, Sejnowski TJ (1995): An information-maximization approach to blind separation and blind deconvolution. Neural Comput 7:1129–1159.

Biswal B, Yetkin FZ, Haughton VM, Hyde JS (1995): Functional connectivity in the motor cortex of resting human brain using echo-planar MRI. Magn Reson Med 34:537–541.

Buckner RL, Andrews-Hanna JR, Schacter DL (2008): The brain's default network: Anatomy, function, and relevance to disease. Ann N Y Acad Sci 1124:1–38.

Calhoun VD, Adali T, Pearlson GD, Pekar JJ (2001): A method for making group inferences from functional MRI data using independent component analysis. Hum Brain Mapp 14:140–151.

Calhoun VD, Miller R, Pearlson G, Adali T (2014): The chronnectome: Time-varying connectivity networks as the next frontier in fMRI data discovery. Neuron 84:262–274.

Chang C, Glover GH (2010): Time-frequency dynamics of resting-state brain connectivity measured with fMRI. Neuroimage 50: 81–98.

Cohen J, Cohen P, West SG, Aiken LS (2013): Applied Multiple Regression/Correlation Analysis For the Behavioral Sciences. London: Routledge.

Cohn MD, Pape LE, Schmaal L, van den Brink W, van Wingen G, Vermeiren RR, Doreleijers TA, Veltman DJ, Popma A (2015): Differential relations between juvenile psychopathic traits and resting state network connectivity. Hum Brain Mapp 36: 2396–2405.

Cole MW, Schneider W (2007): The cognitive control network: Integrated cortical regions with dissociable functions. Neuroimage 37:343–360.

Cordes D, Haughton VM, Arfanakis K, Wendt GJ, Turski PA, Moritz CH, Quigley MA, Meyerand ME (2000): Mapping functionally related regions of brain with functional connectivity MR imaging. AJNR Am J Neuroradiol 21:1636–1644.

Cui Z, Xia Z, Su M, Shu H, Gong G (2016): Disrupted white matter connectivity underlying developmental dyslexia: A machine learning approach. Hum Brain Mapp 37:1443–1458.

Damaraju E, Allen EA, Belger A, Ford JM, McEwen S, Mathalon DH, Mueller BA, Pearlson GD, Potkin SG, Preda A, Turner JA, Vaidya JG, van Erp TG, Calhoun VD (2014): Dynamic functional connectivity analysis reveals transient states of dysconnectivity in schizophrenia. Neuroimage Clin 5:298–308.

Damoiseaux JS, Rombouts SA, Barkhof F, Scheltens P, Stam CJ, Smith SM, Beckmann CF (2006): Consistent resting-state networks across healthy subjects. Proc Natl Acad Sci U S A 103: 13848–13853.

Efron B (1983): Estimating the error rate of a prediction rule: Improvement on cross-validation. J Am Stat Assoc 78: 316–331.

Engel J (2001): A proposed diagnostic scheme for people with epileptic seizures and with epilepsy: Report of the ILAE Task Force on Classification and Terminology. Epilepsia 42: 796–803.

Fan RE, Chang KW, Hsieh CJ, Wang XR, Lin CJ (2008): LIBLINEAR: A library for large linear classification. J Mach Learn Res 9:1871–1874.

Fang P, An J, Zeng LL, Shen H, Chen F, Wang W, Qiu S, Hu D (2015): Multivariate pattern analysis reveals anatomical connectivity differences between the left and right mesial temporal lobe epilepsy. Neuroimage Clin 7:555–561.

Focke NK, Yogarajah M, Symms MR, Gruber O, Paulus W, Duncan JS (2012): Automated MR image classification in temporal lobe epilepsy. Neuroimage 59:356–362.

Fox MD, Snyder AZ, Vincent JL, Corbetta M, Van Essen DC, Raichle ME (2005): The human brain is intrinsically organized into dynamic, anticorrelated functional networks. Proc Natl Acad Sci U S A 102:9673–9678.

Friston KJ, Williams S, Howard R, Frackowiak RS, Turner R (1996): Movement-related effects in fMRI time-series. Magn Reson Med 35:346–355.

Gabrieli JD, Ghosh SS, Whitfield-Gabrieli S (2015): Prediction as a humanitarian and pragmatic contribution from human cognitive neuroscience. Neuron 85:11–26.

Gazzaley A, Cooney JW, McEvoy K, Knight RT, D'Esposito M (2005a): Top-down enhancement and suppression of the magnitude and speed of neural activity. J Cogn Neurosci 17: 507–517.

Gazzaley A, Cooney JW, Rissman J, D'Esposito M (2005b): Top-down suppression deficit underlies working memory impairment in normal aging. Nat Neurosci 8:1298–1300.

Grant AC (2005): Interictal perceptual function in epilepsy. Epilepsy Behav 6:511–519.

Greicius M (2008): Resting-state functional connectivity in neuropsychiatric disorders. Curr Opin Neurol 21:424–430.

Guo WB, Liu F, Xue ZM, Xu XJ, Wu RR, Ma CQ, Wooderson SC, Tan CL, Sun XL, Chen JD, Liu ZN, Xiao CQ, Chen HF, Zhao JP (2012): Alterations of the amplitude of low-frequency fluctuations in treatment-resistant and treatment-response depression: A resting-state fMRI study. Prog Neuropsychopharmacol Biol Psychiatry 37:153–160.

Himberg J, Hyvarinen A, Esposito F (2004): Validating the independent components of neuroimaging time series via clustering and visualization. Neuroimage 22:1214–1222.

Hommet C, Sauerwein HC, De Toffol B, Lassonde M (2006): Idiopathic epileptic syndromes and cognition. Neurosci Biobehav Rev 30:85–96.

Hutchison RM, Morton JB (2015): Tracking the brain's functional coupling dynamics over development. J Neurosci 35:6849–6859.

Hutchison RM, Womelsdorf T, Allen EA, Bandettini PA, Calhoun VD, Corbetta M, Della Penna S, Duyn JH, Glover GH, Gonzalez-Castillo J, Handwerker DA, Keilholz S, Kiviniemi V, Leopold DA, de Pasquale F, Sporns O, Walter M, Chang C (2013a): Dynamic functional connectivity: Promise, issues, and interpretations. Neuroimage 80:360–378.

Hutchison RM, Womelsdorf T, Gati JS, Everling S, Menon RS (2013b): Resting-state networks show dynamic functional connectivity in awake humans and anesthetized macaques. Hum Brain Mapp 34:2154–2177.

Jafri MJ, Pearlson GD, Stevens M, Calhoun VD (2008): A method for functional network connectivity among spatially independent resting-state components in schizophrenia. Neuroimage 39:1666–1681.

Jallon P, Latour P (2005): Epidemiology of idiopathic generalized epilepsies. Epilepsia 46 Suppl 9:10–14.

Kiviniemi V, Vire T, Remes J, Elseoud AA, Starck T, Tervonen O, Nikkinen J (2011): A sliding time-window ICA reveals spatial variability of the default mode network in time. Brain Connect 1:339–347.

Kochiyama T, Morita T, Okada T, Yonekura Y, Matsumura M, Sadato N (2005): Removing the effects of task-related motion using independent-component analysis. Neuroimage 25: 802–814.

Kohavi R (1995): A study of cross-validation and bootstrap for accuracy estimation and model selection. In: Proceedings of the 14th International Joint Conference on Artificial Intelligence. pp 1137–1145.

Kong F, Wang X, Song Y, Liu J (2016): Brain regions involved in dispositional mindfulness during resting state and their relation with well-being. Soc Neurosci 11:331–343.

Kopell NJ, Gritton HJ, Whittington MA, Kramer MA (2014): Beyond the connectome: The dynome. Neuron 83:1319–1328.

Kucyi A, Davis KD (2015): The dynamic pain connectome. Trends Neurosci 38:86–95.

Leonardi N, Van De Ville D (2015): On spurious and real fluctuations of dynamic functional connectivity during rest. Neuroimage 104:430–436.

Li YO, Adali T, Calhoun VD (2007): Estimating the number of independent components for functional magnetic resonance imaging data. Hum Brain Mapp 28:1251–1266.

Li S, Yuan X, Pu F, Li D, Fan Y, Wu L, Chao W, Chen N, He Y, Han Y (2014a): Abnormal changes of multidimensional surface features using multivariate pattern classification in amnestic mild cognitive impairment patients. J Neurosci 34:10541–10553.

Li Y, Wee CY, Jie B, Peng Z, Shen D (2014b): Sparse multivariate autoregressive modeling for mild cognitive impairment classification. Neuroinformatics 12:455–469.

Li Q, Cao W, Liao X, Chen Z, Yang T, Gong Q, Zhou D, Luo C, Yao D (2015): Altered resting state functional network connectivity in children absence epilepsy. J Neurol Sci 354:79–85.

Liao R, McKeown MJ, Krolik JL (2006): Isolation and minimization of head motion-induced signal variations in fMRI data using independent component analysis. Magn Reson Med 55: 1396–1413.

Liao W, Mantini D, Zhang Z, Pan Z, Ding J, Gong Q, Yang Y, Chen H (2010): Evaluating the effective connectivity of resting state networks using conditional Granger causality. Biol Cybern 102:57–69.

Liao W, Zhang Z, Mantini D, Xu Q, Ji GJ, Zhang H, Wang J, Wang Z, Chen G, Tian L, Jiao Q, Zang YF, Lu G (2014): Dynamical intrinsic functional architecture of the brain during absence seizures. Brain Struct Funct 219:2001–2015.

Liao X, Yuan L, Zhao T, Dai Z, Shu N, Xia M, Yang Y, Evans A, He Y (2015): Spontaneous functional network dynamics and associated structural substrates in the human brain. Front Hum Neurosci 9:478.

Liu M, Zhang D, Shen D (2012a): Ensemble sparse classification of Alzheimer's disease. Neuroimage 60:1106–1116.

Liu F, Guo W, Yu D, Gao Q, Gao K, Xue Z, Du H, Zhang J, Tan C, Liu Z, Zhao J, Chen H (2012b): Classification of different therapeutic responses of major depressive disorder with

multivariate pattern analysis method based on structural MR scans. PLoS One 7:e40968.
Liu F, Hu M, Wang S, Guo W, Zhao J, Li J, Xun G, Long Z, Zhang J, Wang Y, Zeng L, Gao Q, Wooderson SC, Chen J, Chen H (2012c): Abnormal regional spontaneous neural activity in first-episode, treatment-naive patients with late-life depression: a resting-state fMRI study. Prog Neuropsychopharmacol Biol Psychiatry 39:326–331.
Liu F, Guo W, Liu L, Long Z, Ma C, Xue Z, Wang Y, Li J, Hu M, Zhang J, Du H, Zeng L, Liu Z, Wooderson SC, Tan C, Zhao J, Chen H (2013): Abnormal amplitude low-frequency oscillations in medication-naive, first-episode patients with major depressive disorder: A resting-state fMRI study. J Affect Disord 146:401–406.
Liu F, Wee CY, Chen H, Shen D (2014): Inter-modality relationship constrained multi-modality multi-task feature selection for Alzheimer's Disease and mild cognitive impairment identification. Neuroimage 84:466–475.
Liu F, Guo W, Fouche JP, Wang Y, Wang W, Ding J, Zeng L, Qiu C, Gong Q, Zhang W, Chen H (2015a): Multivariate classification of social anxiety disorder using whole brain functional connectivity. Brain Struct Funct 220:101–115.
Liu F, Xie B, Wang Y, Guo W, Fouche JP, Long Z, Wang W, Chen H, Li M, Duan X, Zhang J, Qiu M (2015b): Characterization of post-traumatic stress disorder using resting-state fMRI with a multi-level parametric classification approach. Brain Topogr 28:221–237.
Liu F, Zhu C, Wang Y, Guo W, Li M, Wang W, Long Z, Meng Y, Cui Q, Zeng L, Gong Q, Zhang W, Chen H (2015c): Disrupted cortical hubs in functional brain networks in social anxiety disorder. Clin Neurophysiol 126:1711–1716.
Liu F, Zhuo C, Yu C (2016): Altered cerebral blood flow covariance network in schizophrenia. Front Neurosci 10:308.
Loring DW, Meador KJ (2004): Cognitive side effects of antiepileptic drugs in children. Neurology 62:872–877.
Lu H, Zuo Y, Gu H, Waltz JA, Zhan W, Scholl CA, Rea W, Yang Y, Stein EA (2007): Synchronized delta oscillations correlate with the resting-state functional MRI signal. Proc Natl Acad Sci U S A 104:18265–18269.
Luo C, Qiu C, Guo Z, Fang J, Li Q, Lei X, Xia Y, Lai Y, Gong Q, Zhou D, Yao D (2011): Disrupted functional brain connectivity in partial epilepsy: A resting-state fMRI study. PLoS One 7: e28196.
Marini C, King MA, Archer JS, Newton MR, Berkovic SF (2003): Idiopathic generalised epilepsy of adult onset: Clinical syndromes and genetics. J Neurol Neurosurg Psychiatry 74: 192–196.
McGill ML, Devinsky O, Kelly C, Milham M, Castellanos FX, Quinn BT, DuBois J, Young JR, Carlson C, French J, Kuzniecky R, Halgren E, Thesen T (2012): Default mode network abnormalities in idiopathic generalized epilepsy. Epilepsy Behav 23: 353–359.
Oldfield RC (1971): The assessment and analysis of handedness: The Edinburgh inventory. Neuropsychologia 9:97–113.
Power JD, Mitra A, Laumann TO, Snyder AZ, Schlaggar BL, Petersen SE (2014): Methods to detect, characterize, and remove motion artifact in resting state fMRI. Neuroimage 84: 320–341.
Power JD, Schlaggar BL, Petersen SE (2015): Recent progress and outstanding issues in motion correction in resting state fMRI. Neuroimage 105:536–551.
Rabinovich MI, Friston KJ, Varona P (2012): Principles of Brain Dynamics: Global State Interactions. Cambridge: MIT Press.
Raichle ME (2015): The brain's default mode network. Annu Rev Neurosci 38:433–447.
Raichle ME, MacLeod AM, Snyder AZ, Powers WJ, Gusnard DA, Shulman GL (2001): A default mode of brain function. Proc Natl Acad Sci U S A 98:676–682.
Rashid B, Damaraju E, Pearlson GD, Calhoun VD (2014): Dynamic connectivity states estimated from resting fMRI Identify differences among Schizophrenia, bipolar disorder, and healthy control subjects. Front Hum Neurosci 8:897.
Sakoglu U, Pearlson GD, Kiehl KA, Wang YM, Michael AM, Calhoun VD (2010): A method for evaluating dynamic functional network connectivity and task-modulation: Application to schizophrenia. Magn Reson Mater Phys 23:351–366.
Shakil S, Lee CH, Keilholz SD (2016): Evaluation of sliding window correlation performance for characterizing dynamic functional connectivity and brain states. Neuroimage 133: 111–128.
Shen K, Hutchison RM, Bezgin G, Everling S, McIntosh AR (2015): Network structure shapes spontaneous functional connectivity dynamics. J Neurosci 35:5579–5588.
Shen H, Li Z, Qin J, Liu Q, Wang L, Zeng LL, Li H, Hu D (2016): Changes in functional connectivity dynamics associated with vigilance network in taxi drivers. Neuroimage 124:367–378.
Shi J, Zhou S, Liu X, Zhang Q, Lu M, Wang T (2016): Stacked deep polynomial network based representation learning for tumor classification with small ultrasound image dataset. Neurocomputing 194:87–94.
Song M, Du H, Wu N, Hou B, Wu G, Wang J, Feng H, Jiang T (2011): Impaired resting-state functional integrations within default mode network of generalized tonic-clonic seizures epilepsy. PLoS One 6:e17294.
Sporns O (2011): The non-random brain: Efficiency, economy, and complex dynamics. Front Comput Neurosci 5:5.
Su L, An J, Ma Q, Qiu S, Hu D (2015): Influence of resting-state network on lateralization of functional connectivity in mesial temporal lobe epilepsy. AJNR Am J Neuroradiol 36: 1479–1487.
Sullivan JE, Dlugos DJ (2004): Idiopathic generalized epilepsy. Curr Treat Options Neurol 6:231–242.
Thung KH, Wee CY, Yap PT, Shen D (2014): Neurodegenerative disease diagnosis using incomplete multi-modality data via matrix shrinkage and completion. Neuroimage 91:386–400.
Tomasi D, Volkow ND (2011): Association between functional connectivity hubs and brain networks. Cereb Cortex 21: 2003–2013.
Tzourio-Mazoyer N, Landeau B, Papathanassiou D, Crivello F, Etard O, Delcroix N, Mazoyer B, Joliot M (2002): Automated anatomical labeling of activations in SPM using a macroscopic anatomical parcellation of the MNI MRI single-subject brain. Neuroimage 15:273–289.
Van den Heuvel MP, Hulshoff Pol HE (2010): Exploring the brain network: A review on resting-state fMRI functional connectivity. Eur Neuropsychopharmacol 20:519–534.
Van den Heuvel MP, Sporns O (2013): Network hubs in the human brain. Trends Cogn Sci 17:683–696.
Von der Malsburg C, Phillips WA, Singer W (2010): Dynamic Coordination in the Brain: From Neurons to Mind. Cambridge: MIT Press.
Wang Z, Lu G, Zhang Z, Zhong Y, Jiao Q, Tan Q, Tian L, Chen G, Liao W, Li K, Liu Y (2011): Altered resting state networks in epileptic patients with generalized tonic-clonic seizures. Brain Res 1374:134–141.

Wang J, Zuo X, Dai Z, Xia M, Zhao Z, Zhao X, Jia J, Han Y, He Y (2013): Disrupted functional brain connectome in individuals at risk for Alzheimer's disease. Biol Psychiatry 73: 472–481.

Wang L, Liu Q, Shen H, Li H, Hu D (2015): Large-scale functional brain network changes in taxi drivers: Evidence from resting-state fMRI. Hum Brain Mapp 36:862–871.

Wang X, Fang Y, Cui Z, Xu Y, He Y, Guo Q, Bi Y (2016a): Representing object categories by connections: Evidence from a mutivariate connectivity pattern classification approach. Hum Brain Mapp 37:3685–3697.

Wang X, Song Y, Zhen Z, Liu J (2016b): Functional integration of the posterior superior temporal sulcus correlates with facial expression recognition. Hum Brain Mapp 37:1930–1940.

Yan CG, Cheung B, Kelly C, Colcombe S, Craddock RC, Di Martino A, Li Q, Zuo XN, Castellanos FX, Milham MP (2013): A comprehensive assessment of regional variation in the impact of head micromovements on functional connectomics. Neuroimage 76:183–201.

Zalesky A, Breakspear M (2015): Towards a statistical test for functional connectivity dynamics. Neuroimage 114:466–470.

Zalesky A, Fornito A, Bullmore ET (2010): Network-based statistic: Identifying differences in brain networks. Neuroimage 53: 1197–1207.

Zeng LL, Shen H, Liu L, Wang L, Li B, Fang P, Zhou Z, Li Y, Hu D (2012): Identifying major depression using whole-brain functional connectivity: A multivariate pattern analysis. Brain 135:1498–1507.

Zeng LL, Shen H, Liu L, Hu D (2014): Unsupervised classification of major depression using functional connectivity MRI. Hum Brain Mapp 35:1630–1641.

Zhang Z, Lu G, Zhong Y, Tan Q, Liao W, Chen Z, Shi J, Liu Y (2009): Impaired perceptual networks in temporal lobe epilepsy revealed by resting fMRI. J Neurol 256:1705–1713.

Zhang J, Cheng W, Wang Z, Zhang Z, Lu W, Lu G, Feng J (2012): Pattern classification of large-scale functional brain networks: Identification of informative neuroimaging markers for epilepsy. PLoS One 7:e36733.

Zhang Y, Liu F, Chen H, Li M, Duan X, Xie B (2015): Intranetwork and internetwork functional connectivity alterations in post-traumatic stress disorder. J Affect Disord 187:114–121.

Zhang J, Cheng W, Liu Z, Zhang K, Lei X, Yao Y, Becker B, Liu Y, Kendrick KM, Lu G, Feng J (2016): Neural, electrophysiological and anatomical basis of brain-network variability and its characteristic changes in mental disorders. Brain 139:2307–2321.

Zhu X, Suk HI, Shen D (2014): A novel matrix-similarity based loss function for joint regression and classification in AD diagnosis. Neuroimage 100:91–105.

Zuo XN, Kelly C, Adelstein JS, Klein DF, Castellanos FX, Milham MP (2010): Reliable intrinsic connectivity networks: Test-retest evaluation using ICA and dual regression approach. Neuroimage 49:2163–2177.